Title: **Cortical neural activity predicts sensory acuity under optogenetic manipulation.**

Authors: Briguglio, J. J.[1], Aizenberg, M.[2], Balasubramanian, V.[1], Geffen, M.N.[2]

Affiliations: 1. Department of Physics, 2. Department of Otorhinolaryngology: HNS, Department of Neuroscience, University of Pennsylvania, Philadelphia, PA

Corresponding author:

Maria N. Geffen

Department of Otorhinolaryngology: HNS
University of Pennsylvania
5 Ravdin
3400 Spruce St.
Philadelphia PA 19104

Tel.: 215.898.0782
Fax: 215.898.9994
Email: mgeffen@med.upenn.edu

Abstract.

Excitatory and inhibitory neurons in the mammalian sensory cortex form interconnected circuits controlling cortical stimulus selectivity, but their relation to sensory acuity remains unknown. Here we show that the behavioral alteration of frequency discrimination acuity in mice due to optogenetic activation and suppression of auditory cortex (AC) neurons varies from animal to animal in both magnitude and sign. We used Fisher information based on recordings from AC neural populations to estimate the behavioral discrimination acuity under different optogenetic conditions, and showed that the changes in population tuning consistently predict the changes in behavior for each individual separately. The strong correlation between cortical and behavioral changes demonstrates that AC facilitates frequency discrimination in a manner predicted by optimal decoding from cortical neurons. This suggests that diversity in auditory behavior may be partly explained by variations in the circuit properties of AC, consistent with theoretical prediction for balanced excitatory-inhibitory networks.

Introduction.

Individual differences give rise to diversity—an essential feature of the success of many species. Uncovering how differences in neural activity lead to differences in behavior is crucial to developing an understanding of brain function that applies to a population with diverse behaviors. We noted from previous studies that individual mice vary markedly in their ability to discriminate nearby tones (Kurt and Ehret, 2010; Aizenberg and Geffen, 2013; Aizenberg et al., 2015; Mwilambwe-Tshilobo et al., 2015).   This acuity should rely on frequency tuning of neurons in the auditory pathway. It is known that frequency tuning in auditory cortex (AC) is determined by interactions in the excitatory-inhibitory network (Chen and Jen, 2000; Wang et al., 2000; Wang et al., 2002a; Wehr and Zador, 2003; Oswald et al., 2006; Wu et al., 2008; Tan and Wehr, 2009; Seybold et al., 2015; Phillips and Hasenstaub, 2016). Theoretical work on balanced excitatory-inhibitory networks has shown that driving inputs to inhibitory units can lead to either a decrease or an increase of excitatory responses, depending on the specifics of excitatory and inhibitory recurrent connections or the strength of inhibitory manipulations (Tsodyks et al., 1997).   We hypothesized that changes in cortical circuit interactions could underlie changes in tone discrimination behavior, and that variation in these interactions could be the locus of differences in frequency discrimination behavior among individuals. To test these hypotheses, we manipulated activity of excitatory and inhibitory neurons in AC optogenetically, and showed that differences in behavioral frequency discrimination across mice during optogenetic manipulations are predicted by changes in the tone responses of neurons.

Recent experiments support the view that the auditory cortex plays a causally modulatory function in frequency discrimination.   Neurons in the AC exhibit selectivity for the frequency of a stimulus, which can be changed by learning (Recanzone et al., 1992; Kilgard and Merzenich, 2002; Fritz et al., 2003; Fritz et al., 2005; Polley et al., 2006; Froemke et al., 2013; Znamenskiy and Zador, 2013). Pharmacological suppression of the auditory cortex (Talwar and Gerstein, 2001) and lesions of AC in humans patients (Tramo et al., 2002) can impair frequency discrimination, although other lesioning(Ohl et al., 1999) and pharmacological (Gimenez et al., 2015) studies have only shown small effects.   Recently, we found that pharmacological suppression of neural activity in AC abolished learning-driven changes in frequency discrimination acuity (Aizenberg and Geffen, 2013). In addition, optogenetic activation of spiking activity of parvalbumin-positive inhibitory neurons (PVs) on average improved behavioral frequency discrimination acuity, while optogenetic suppression impaired it (Aizenberg et al., 2015).   Taken together, these recent studies suggest that while AC may not be necessary for frequency discrimination, it plays an important modulatory role.

Here, to quantify the role of AC in frequency discrimination, we recorded tone-evoked responses from populations of cortical neurons in mice and measured their frequency discrimination acuity, while

manipulating activity of excitatory or inhibitory neuronal populations in AC. We developed a novel method using Fisher Information to obtain a neurometric estimate for the tone discrimination threshold from the recorded neurons. Cortical recordings necessarily sub-sample the population of neurons. So rather than trying to explain the absolute discrimination threshold, we made a differential measurement to ask whether changes in the neurometric threshold upon optogenetic manipulation predicted changes in the behavioral threshold. We used three different manipulations (activation of pyramidal cells, and activation or suppression of PV interneurons) to compare changes in the animal's behavior to changes in neuronal activity. These differences may arise from intrinsic differences in cortical circuitry or from variable strength of the optogenetic manipulation across animals. Strikingly, the same manipulation sometimes produced opposite changes in the behavior of individuals. The optogenetic interventions also led to changes in tone-evoked responses of recorded neurons. Computational analysis predicted consequent changes in the discrimination thresholds, which explained the measured behavioral changes, including cases where individuals responded oppositely.

Our results support the view that the spectral representation in AC modulates frequency discrimination acuity, and suggests that diversity in auditory behavior partly stems from variations in the excitatory-inhibitory interactions in the auditory cortex.

Results.

Measuring frequency discrimination acuity.

To measure frequency discrimination acuity, we used a procedure based on pre-pulse inhibition of the acoustic startle reflex (Figure 1A, B). Like other mammals, mice startle to loud noise. The startle response, as measured by the change in pressure exerted by the subject on a balance platform, is typically decreased when the startle noise is preceded by a brief tone that mice can detect – a phenomenon termed pre-pulse inhibition (PPI). We presented mice with a continuous tone at one frequency, which was stepped to a tone of a different frequency just prior to the startle noise. The startle response was attenuated as the frequency difference between background and pre-pulse tones increased (Figure 1B, C). This attenuation reflects the ability of the mouse to detect frequency differences (Aizenberg and Geffen, 2013; Aizenberg et al., 2015). We characterized frequency discrimination acuity in terms of a *behavioral threshold* – the frequency difference that produced 50% of the maximum PPI (Figure 1 C).
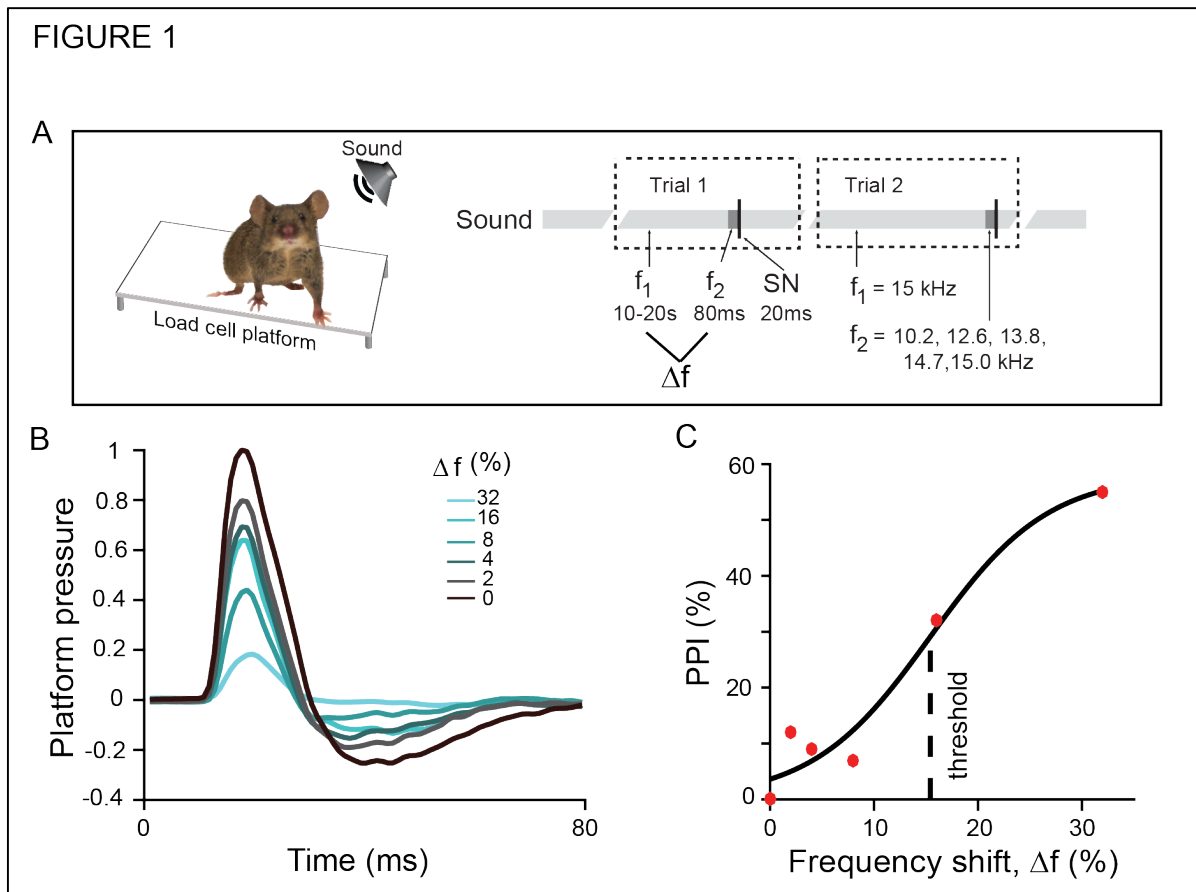
FIGURE 1

Figure 1: Measurement of behavioral frequency discrimination acuity.
A. Schematic of measurement of frequency discrimination acuity in mouse. **Left**: Startle response is measured as pressure the subject exerts on a platform. **Right**: Sound stimulus time course: an ongoing background tone (light gray, f_1) is followed by a brief pre-pulse tone of different frequency (dark grey band, f_2,) and then by a startle noise (thin black band, SN).
B. Normalized time course of platform pressure during the startle response to noise for different pre-pulse tones for an exemplar mouse.
C. Pre-pulse inhibition measured as reduction in the acoustic startle response as a function of the frequency shift (Δf) between the background and pre-pulse tones (see Methods for definition) of an exemplar mouse. Dots: data, solid line: fit.

Neurometric discrimination thresholds from Fisher Information

Next, we recorded the activity of putative excitatory cells (Methods) in AC, while presenting the awake head-fixed mouse with a random tone pip stimulus (50 ms tone pips presented every 500 ms, frequency changed at random, Figure 2A). For each frequency-tuned neuron, we measured frequency response curves (mean firing rate as a function of tone frequency, Methods and Figure 2B). To estimate a discrimination threshold from the frequency-tuned neural population recorded in each mouse we used Fisher Information analysis. To do so, we fit Gaussian functions to the response curve of each neuron, and assumed that neurons responded independently and with Poisson variability. Standard methods then provided the Fisher information for frequency discrimination based

Page 4

on the population response (Methods; Figure 2C) (Cover and Thomas, 1991). Fisher information quantifies the amount of information that neural responses provide to distinguish nearby frequencies. Decoding sensitivity increases with Fisher information. Since this information is large when the neural response changes quickly as a function of frequency, it is higher on the slopes of the tuning curves than in the center.

The inverse square root of the Fisher Information bounds the accuracy with which nearby frequencies can be distinguished based on population activity. This quantity is by definition the *neurometric threshold*, and gives the frequency difference that can be discriminated with 70% accuracy. Figure 2D shows the neurometric thresholds determined in an individual mouse on the basis of the neural population recorded in its cortex.

A direct comparison of the neurometric threshold with behavior faces three challenges: (a) Discrimination accuracy need not translate linearly into thresholds determined from the pre-pulse inhibition of the acoustic startle response measured here, (b) Cortical recordings inevitably sub-sample the population of responsive neurons, and (c) Frequency discrimination is supported by multiple pathways, some of which may not involve the auditory cortex. In general, we expect the neurometric thresholds computed here to be higher than the behavioral thresholds, because of the limited number of recorded neurons (e.g., Figure 2D).

In view of these challenges we did not seek to predict absolute behavioral thresholds from the population of recorded frequency-tuned neurons. Rather, we manipulated the cortex optogenetically, and tested whether there was a correlation between the resulting changes in the neurometric estimate of discrimination thresholds and corresponding changes in behavior.
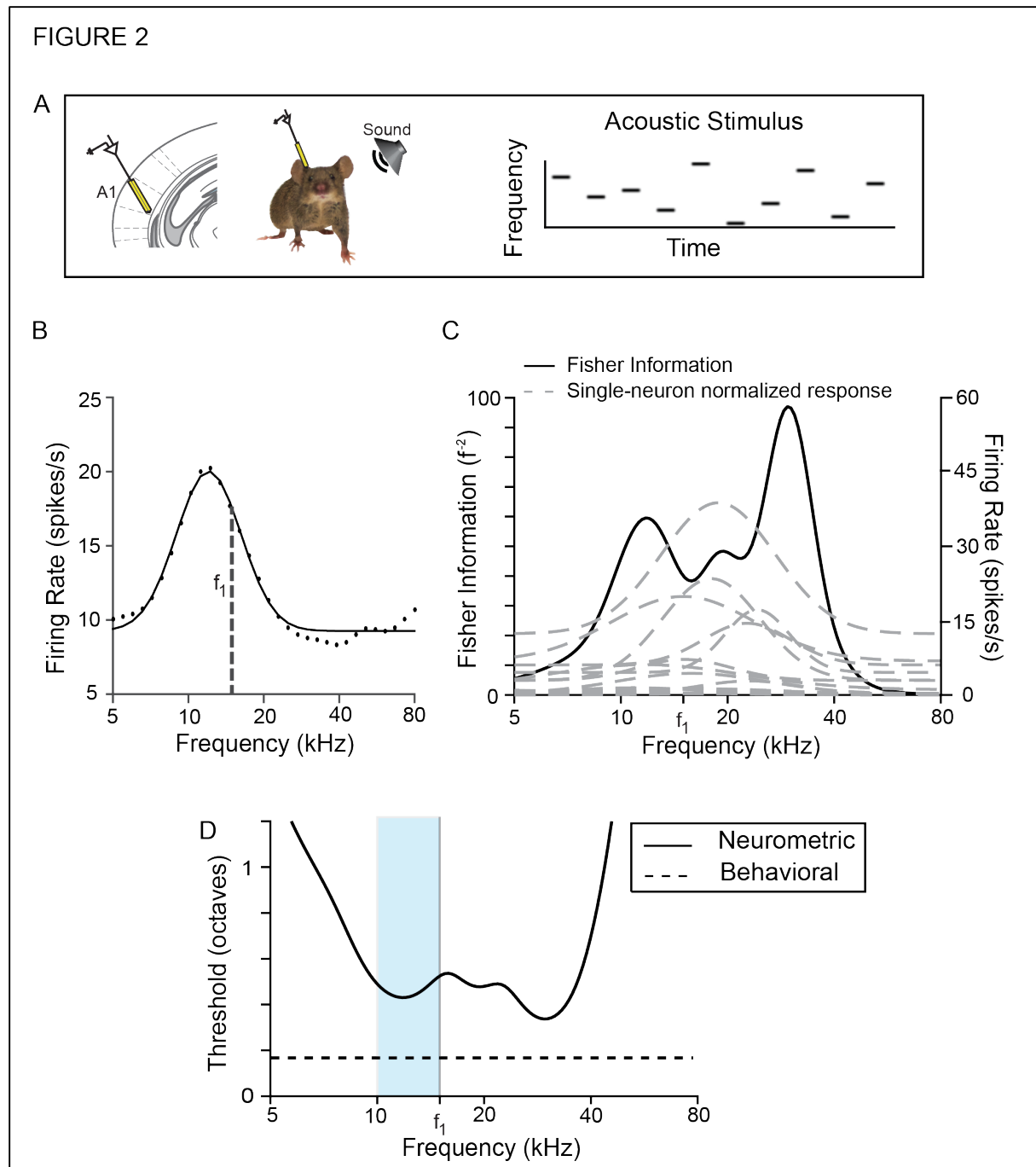
FIGURE 2

Figure 2: Measurement of neurometric frequency discrimination acuity.

A. **Left**: Schematic of electrophysiological recording of neuronal responses in the primary auditory cortex (A1) in awake mouse. **Right**: The stimulus consists of a pseudorandom sequence of pure tones at varying frequency and intensity levels.

B. Representative frequency response function for a single neuron (f_1 = background tone in Fig. 1). Black dots: data, black line: fit.

C. Fisher information for tone discrimination (black) computed on the basis of frequency response functions (gray dashed) of neurons recorded in the same mouse.

D. Neurometric threshold for decoding frequency (solid) computed on the basis of the inverse square root of Fisher Information computed in **C**. The neurometric threshold based on the recorded population lies above behavioral threshold for discrimination around f_1 (dashed line). Light blue band indicates the region in frequency space from which behavioral measurements were taken.

Optogenetically induced changes in neurometric and behavioral thresholds are correlated.

Frequency tuning of AC neurons is thought to depend on the combination of excitatory and inhibitory inputs (Chen and Jen, 2000; Wang et al., 2000; Wang et al., 2002a; Wehr and Zador, 2003; Aizenberg et al., 2015). To manipulate tone responses of AC neurons, we targeted the most common interneuron subtype, parvalbumin-positive interneurons (PVs). We drove PVs to express Archaerhodopsin (Arch) or Channelrhodopsin (ChR2) by injecting a floxed Arch- or ChR2- encoding virus in PV-Cre mice. We verified the efficiency of the viral transfection and light stimulation by measuring the effect of light on spontaneous firing rates of neurons. As expected, when PVs were activated by light, thus increasing inhibition, spontaneous activity decreased in the recorded population (Figure 3A) (Natan et al., 2015). Optogenetically suppressing PVs had the opposite effect: the spontaneous rate of most recorded neurons increased (Figure 3B). We also drove excitatory neurons in AC to express ChR2 and found that optogenetic illumination of AC led to an elevated spontaneous firing rate (Figure 3C). Thus, we reliably used light to manipulate the activity of excitatory and PV neurons in AC.

We next measured the behavioral effects of manipulating neural activity in AC. In half of the trials, we illuminated AC at the same time as providing the pre-pulse stimulus. Activating PVs (Figure 3D) decreased the threshold for most animals (N=5) and increased it for some (N=2), while a few (N=4) did not have a statistically significant threshold change. Suppressing PVs (Figure 3E) produced an increase in the frequency discrimination threshold for two animals, and did not produce statistically significant change for one animal. Optogenetically activating excitatory neurons increased the threshold for most animals (N=3) and decreased it for one, with one animal displaying no threshold change (Figure 3F). For several animals, (N=7) the manipulations did not produce any significant behavioral changes.

Finally, we measured the effect of manipulating neuronal activity on the neurometric frequency discrimination thresholds predicted from the recorded population. Activating PVs led to a decrease in the predicted threshold (Figures 3G, 4A, B, blue) for most animals (N=7) and an increase for some (N=2). The predicted threshold increased for most animals (N=3) after suppressing PVs (Figures 3H, 4A, B green), but decreased for two. Activating excitatory neurons (Figures 3I, 4A, B, red) increased the predicted threshold for all animals (N=3). There was no predicted change for two animals (<2% change in predicted threshold).

For most individuals (N=15/19) and on average, the sign of the neurometric change in threshold matched the sign of the change in behavioral threshold (Figure 4A, B). This qualitative agreement was striking, given that the electrical recordings only sample a few neurons, while the light has a global effect on the auditory cortex and sometimes leads to opposite behavioral changes. To quantify

the correlation, we compared the neurometric and behavioral frequency discrimination thresholds for each mouse, under light-on and light-off conditions. The number of recorded tone-responsive
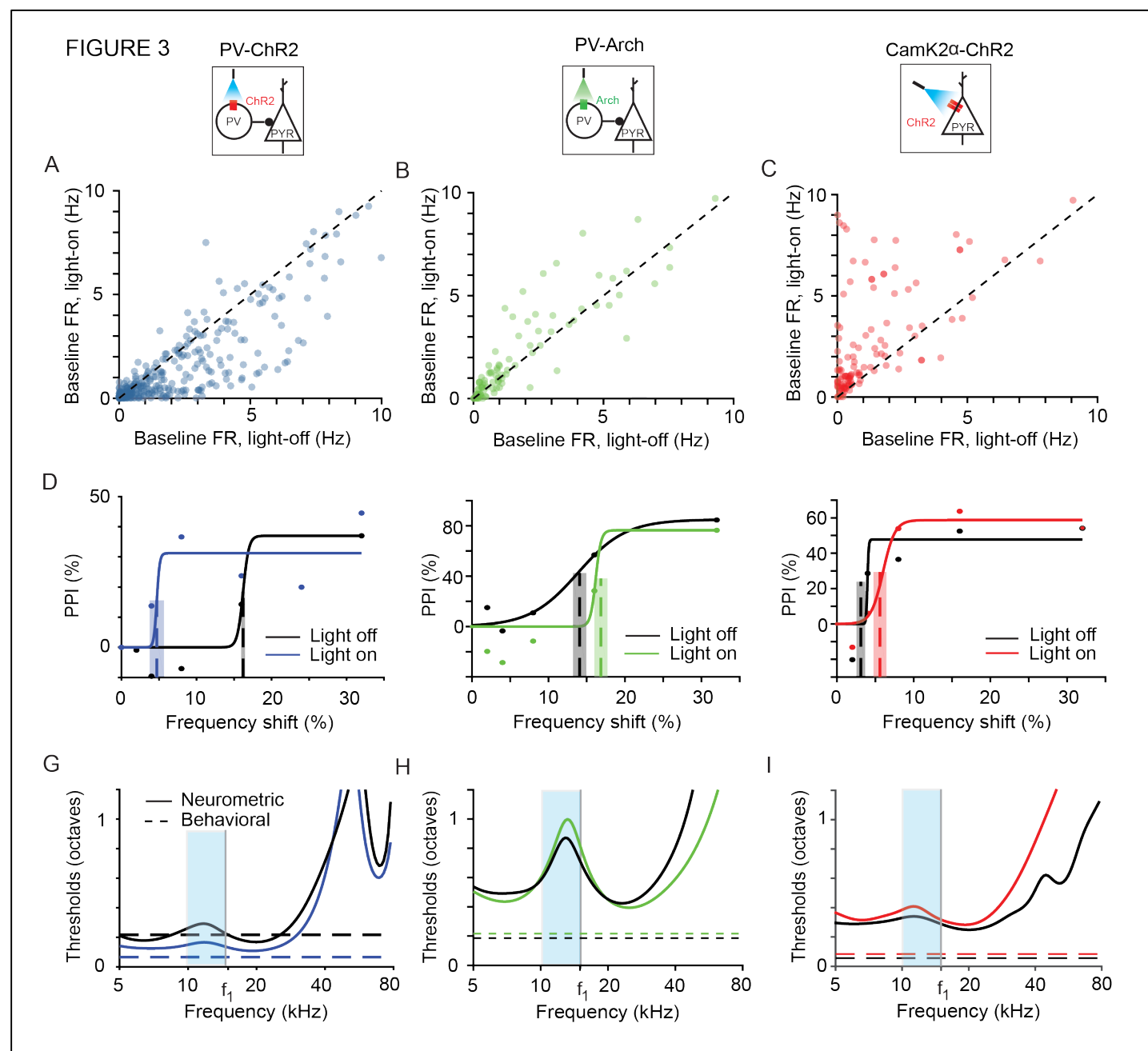

Figure 3: Optogenetic manipulation of PV activity shifts behavioral and neurometric frequency discrimination thresholds.

A,B,C: Baseline firing rate of light-on versus light-off trials for all frequency-tuned neurons pooled across subjects in PV-ChR2 (Blue), PV-Arch (Green), CamK2a-ChR2 (Red) mice, respectively. **D,E,F**: PPI as a function of tone frequency shift for exemplar mice. Best estimated thresholds (dashed lines) and uncertainties (overlaid gray rectangle) are plotted for reference. Black: light-off trials; Blue, Green, Red: light-on trials. Dots: data, solid lines: best fit curve. **G,H,I**: Neurometric threshold estimate as inverse square root of Fisher information (solid) and behavioral threshold at f_1, (horizontal dotted) for the same mice as **D,E,F**. Light blue bands indicate the region in frequency space from which behavioral measurements were taken.

neurons varied significantly between mice (14-104 per animal). Using the linear dependence of the Fisher Information on population size we estimated that ~1000 independent neurons would be necessary for the neurometric thresholds to match the absolute behavioral thresholds (see Methods). Therefore, in order to compare across animals, we divided the Fisher Information computed from the population by the number of neurons, and then scaled the result back linearly to an effective population size of 1000 neural units.
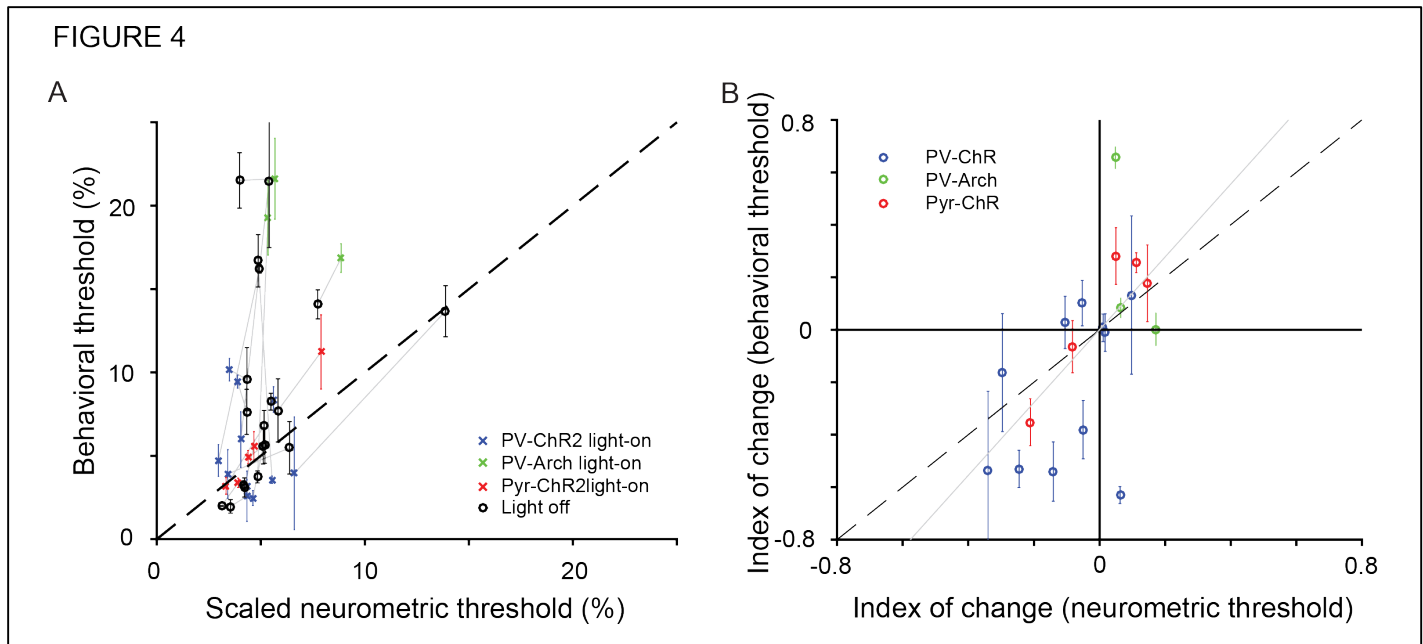

FIGURE 4

Figure 4. Changes in A1 tone responses due to optogenetic manipulations predict changes in behavioral frequency discrimination acuity across individuals.

A. Behavioral versus scaled neurometric frequency discrimination thresholds. Neurometric threshold is scaled to an effective population size of 1000 neurons to control for differences in numbers of measured neurons. The scaled neurometric threshold based on the small recorded population was significantly (but weakly so, C=.37, p=0.02) correlated with the behavioral threshold. Each of 19 mice contributes 2 data points, representing the light-on and light-off conditions. Gray lines connect light-on and light-off points for a single mouse.

B. The index of change in neurometric threshold (difference in light on vs. off thresholds divided by the sum) was strongly correlated with the behavioral frequency discrimination (Correlation coefficient = 0.59, p=0.007). There is one data point for each mouse. Gray line is the best fit line through the origin. Behavioral errors were computed as described in the Methods.

We compared the resulting estimate to the behavioral threshold (Figure 4, Figure 4 – Figure Supplement 2). We first found a correlation between the absolute behavioral and neurometric thresholds under all conditions (Figure 4A). The correlation is statistically significant ($C = .37$, $p = .02$, $N = 38$, including a light-on and a light-off measurement for each of 19 mice), but only weakly so (i.e. *p>0.01*), probably because our recordings sub-sample the population of neurons involved in frequency discrimination. To test more closely the effect of the optogenetic manipulations, we

computed an index of change as the difference in thresholds before and after application of light, divided by the sum. We found that index of change of the neurometric thresholds was strongly correlated with the behaviorally measured index of change in frequency discrimination acuity threshold (Figure 4B, $C = .59$, $p = .007$, $N = 19$).

These correlations suggest that: (a) auditory cortex does modulate frequency discrimination behavior, (b) the effects seen in the small recorded patch are representative, and (c) individual differences in auditory behavior are directly driven by differences in excitatory and inhibitory interactions in cortical circuits.

Mouse	Type	Behavior						Neurometric (scaled)			Neurons
		T_{off} (%)	ΔT_{off} (%)	T_{on} (%)	ΔT_{on} (%)	I_{change}	ΔI_{change}	T_{off} (%)	T_{on} (%)	I_{change}	
1	PV-Arch	21.5	1.7	22	2	0.00	.06	6.4	9.1	.17	42
2	PV-ChR2	16.2	.3	4.7	.1	-.53	.07	7.9	4.7	-.25	104
3	PV-ChR2	22	4	6.0	1.7	-.54	.11	8.7	6.5	-.14	16
4	PV-ChR2	13.7	1.5	4	3	-.54	.3	22.8	10.6	-.34	20
5	PV-ChR2	16.7	1.6	3.6	.2	-.63	.03	7.8	8.9	.06	24
6	PV-ChR2	5.6	1.1	2.5	.5	-.38	.11	8.2	7.4	-.05	25
7	PV-Arch	3.7	.4	19	2	.66	.04	7.8	8.6	.05	25
8	PV-Arch	14.1	.9	16.9	9	.08	.04	12.5	14.4	.07	23
9	Pyr-ChR2	5.6	1.1	4.9	.4	-.06	.1	8.3	7.0	-.08	19
10	Pyr-ChR2	6.8	.9	3.2	.5	-.35	.09	8.3	5.3	-.21	16
11	Pyr-ChR2	.7	1.9	11	2	.18	.15	9.4	12.8	.15	23
12	Pyr-ChR2	2.0	.01	3.4	.3	.26	.04	5.0	6.3	.11	26
13	Pyr-ChR2	3.1	.6	5.6	.9	.28	.11	6.7	7.5	.05	43
14	PV-ChR2	3.2	.3	3.2	.4	-.01	.07	6.7	6.9	.02	34
15	PV-ChR2	5.5	1.6	3.9	1.5	-.16	.23	10.3	5.5	-.3	16
16	PV-ChR2	9.6	1.9	10.2	.7	.03	.10	.9	5.6	-.11	14
17	PV-ChR2	2.0	.4	2.6	1.5	.13	.30	5.7	6.9	.10	15
18	PV-ChR2	7.6	1.4	9.5	.4	.10	.09	6.9	6.2	-.05	22
19	PV-ChR2	8.3	.5	8.4	.8	.01	.05	8.8	9.0	.01	39

Figure 4 – Figure Supplement 1: Table containing relevant measured thresholds, index of change values, neuron number, and type of mouse used.

Controls: effects of optogenetic manipulation on neural variability and correlations

Our model makes two assumptions that could be violated in neural systems: that cortical neurons obey Poisson statistics and that neural responses are independent of one another. In order to test the first assumption in our data, we measured the Fano factor of the recorded neurons. A large Fano factor indicates high neuronal variability (Blackwell et al., 2016). The average Fano factor was around 1.2, similar to the value expected for Poisson neurons and to that previously measured across different cortical areas (Churchland et al., 2010). We found that none of the three optogenetic manipulations (PV-ChR2: $t_{335} = .4$, $p = .69$; PV-Arch: $t_{89} = .92$, $p = .36$; Pyr-ChR2: $t_{133} = -.2$, $p =$

.84; Figure 5A-C) had a systematic effect on the distribution of Fano factors. This justified our analysis where neurons were treated as Poisson, both with and without optogenetic manipulation.
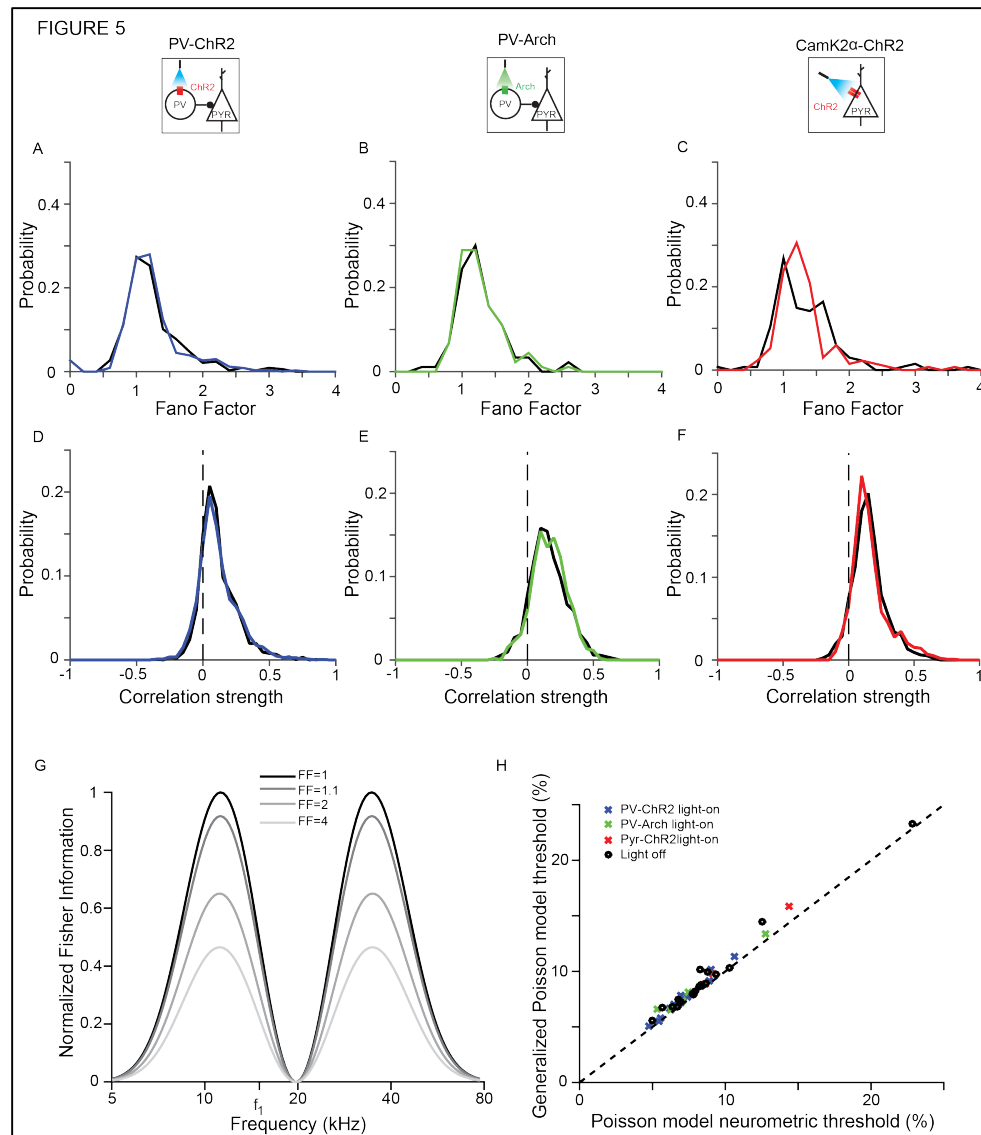

Figure 5. Optogenetic manipulations do not change neuronal variability or correlations.
A-C. Fano factor pooled across mice distributions are similar under light-on and light-off conditions. A: PV-ChR2, B: PV-Arch, C: CamK2a-ChR2. Black: light-off trials; Blue, Green, Red: light-on trials. Dots
D-F. Pairwise correlation distributions pooled across mice are similar under light-on and light-off conditions. D: PV-ChR2, E: PV-Arch, F: CamK2a-ChR2. Colors same as in A.
G. Increasing Fano factor reduces Fisher Information, shown here for a single neuron with Gaussian tuning curve (amplitude = 8 spikes/s, center frequency 20kHZ, tuning width = 0.2 decades) with a constant baseline (2 spikes/s).
H. Incorporating the measured Fano factors into our model of neuronal firing via a generalized Poisson model has a weak effect on the predicted threshold.

We next considered that neural variability has been observed to increase with the activity level of neurons (Goris et al., 2014). It is plausible that the most active neurons, which have the largest impact on Fisher information, may be more variable than expected from the average Fano factor

value. The Fisher information decreases as the Fano factor increases (Figure 5G), so higher variability in the most active neurons would disproportionately decrease the neurometric discriminability. To test whether this might be the case, we computed the neurometric thresholds using a generalized Poisson noise model that took into account the Fano factor of each recorded neuron separately. Neurometric thresholds using this model changed only slightly from the thresholds computed using the simple Poisson noise model (Figure 5H), again justifying our analysis.

We also measured the strength of pairwise neural correlations, and observed they tended to be small but positive ($\bar{C}_{PV-ChR2} = .09$, $t_{1937} = 28$, $p = 4.6 * 10^{-141}$; $\bar{C}_{PV-Arch} = .13$, $t_{524} = 22$, $p = 2.2 * 10^{-76}$; $\bar{C}_{Pyr-ChR2} = .13$, $t_{982} = 32$, $p = 1.1 * 10^{-155}$). The optogenetic manipulations had no systematic effect on the distribution of correlations (paired t test ns: PV-ChR2 $t_{1937} = .26$, $p = .80$; PV-Arch $t_{524} = -1.3$, $p = .18$; Pyr-ChR2 $t_{982} = -1.7$, $p = .09$; see Figure 5D-F, Figure 5 – Figure Supplement 1). Correlations in similar models have been observed to lead only to small increases in population-level discrimination threshold (Gu et al., 2010). The small changes in threshold observed in previous work, in addition to the negligible change in the correlation distribution that we observe upon optogenetic manipulation, make it unlikely that correlations account for the neurometric threshold changes due to manipulations of cortical activity.
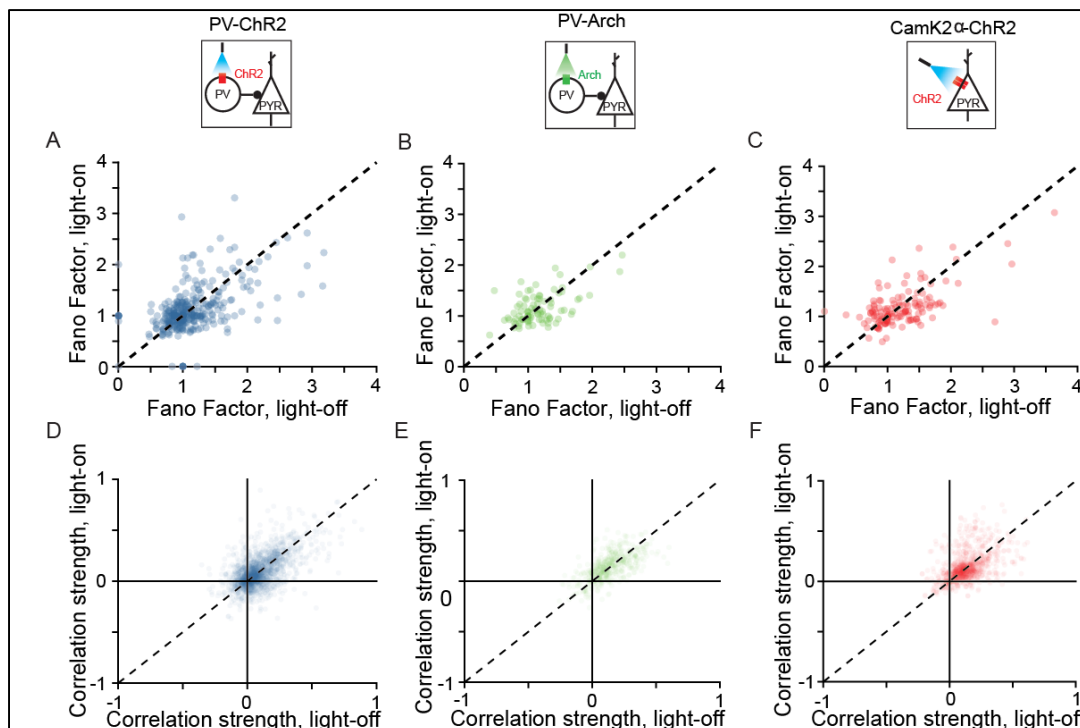

Figure 5 – Figure Supplement 1: Fano factor and correlation scatter plots comparing light-on and light-off conditions. **A-C**: Fano factor with and without light on for PV-ChR2, PV-Arch, and Pyr-ChR2 mice, respectively.
D-F: Pairwise correlations with and without light on for PV-ChR2, PV-Arch, and Pyr-ChR2 mice, respectively.

Discussion.

Theory has shown that providing inputs to inhibitory neurons in a balanced excitatory-inhibitory network can lead to either a decrease, or, paradoxically, an increase of excitatory responses, depending on the specifics of recurrent coupling for excitatory and inhibitory neurons in the network or the strength of inhibitory manipulations (Tsodyks et al., 1997). Indeed, we find that manipulation of the excitatory-inhibitory interactions in auditory cortex drives diverse, and sometimes opposite, changes in tone-evoked responses across individuals. Remarkably, we found a strong correlation between these changes in neuronal populations, and behavioral changes in the acuity of frequency discrimination by individual mice. Thus our results demonstrate a role for excitatory-inhibitory networks in the cortex in the differentiation between individuals, reflecting theoretically predicted dynamics in such systems.

In addition, our results provide insight into the mechanics of cortical inhibition in shaping frequency discrimination behavior. Cortical inhibitory neurons have been hypothesized to modulate numerous aspects of tone-evoked responses in the excitatory cortical circuit, such as tuning width, reliability of firing, tone-evoked response strength, and correlations in firing rate activity (Wang et al., 2000; Wang et al., 2002b; Froemke, 2015). We shed light on these hypotheses by optogenetically manipulating PVs, which are the most common inhibitory subtype, representing 40% of interneurons in the cortex (Rudy et al., 2011; Moore and Wehr, 2013; Li et al., 2015). We found that neither the reliability of firing of excitatory neurons, nor their correlations were systematically affected by modulation of the PV activity. Specifically, the distributions of Fano factors and pairwise correlations were unchanged by our circuit manipulations. PV suppression or activation did affect tone-evoked responses of cortical neurons, including the magnitude of the tone-evoked response and tuning width (Aizenberg et al., 2015).

Our results are thus consistent with the diversity of modulatory effects predicted for inhibition-stabilized networks (Ozeki et al., 2009). In such networks, a strong recurrent inhibitory drive serves to offset the large destabilizing fluctuations in firing rate induced by excitatory recurrence, provided the inhibitory time constants are sufficiently short (Ahmadian et al., 2011). Indeed, modeling responses of auditory cortical neurons demonstrated that recurrent inhibition, either lateralized or co-tuned with excitatory inputs, is required to produce the large variety of response types observed in AC (de la Rocha et al., 2008). Bi-directional modulation of either excitatory or inhibitory dynamics is further amplified by synaptic plasticity in neuronal circuits, in the form of depression or facilitation (Dror and Tsodyks, 2000). Our work has demonstrated that modulating elements of the excitatory-inhibitory network in AC does have diverse effects on neural firing, and that, furthermore, these effects are directly correlated with variations in frequency discrimination behavior.

The limited size of our recordings of 10-100 frequency-tuned neurons per animal precluded direct prediction of behavioral thresholds: an extrapolation from the measured population indicates that O(1000) neurons would be required to fully account for behaviorally observed frequency discrimination threshold (Figure 4 – Figure Supplement 2). This observation is consistent with an anatomical estimate suggesting that O(1000) neurons in the mouse AC are responsive to a given tone (mouse cortex has ~10^5 neurons/mm^3 (Schuz and Palm, 1989), the AC is ~1 mm^3 in size, ~30-50% of neurons are frequency tuned, and the tuning width is ~1/10 of the auditory spectrum). The fact that we were able to make strong predictions about optogenetic effects on behavior despite this sub-sampling suggests that the changes we observed in the measured cortical neurons were representative of changes occurring across the entire AC. This may be partly because our laser simultaneously illuminated the entire structure. Comprehensive recordings of more complete populations of AC neurons will enable a test of the hypothesis that frequency discrimination performance is limited by the encoding at the cortical level.

We have observed a relationship between neural responses and behavior under the specific conditions of optogenetic manipulations of cortex, but the methods used here will be broadly useful for understanding other complex phenomena. For example, appetitive and aversive conditioning has been shown to effect cortical remapping (Bakin and Weinberger, 1990; Recanzone et al., 1993; Polley et al., 2006) and to lead to diverse behavioral responses (Aizenberg and Geffen, 2013; Aizenberg et al., 2015). More specifically, it leads to an overrepresentation of the aversive stimulus in cortex, and while some animals show improved frequency discrimination acuity, others are impaired. Interestingly, different changes in neural responses can lead to improved or impaired acuity, depending on the details of the change (Figure 6). For example, shifting the neural tuning curves towards the aversive frequency leads to increased sensitivity near this tone (Figure 6B), while simply increasing neural activity in response to tones near the aversive frequency can lead to impaired discrimination (Figure 6C). The methods used here can help to understand whether the change in behavioral frequency discrimination can be explained by changes in tuning properties within auditory cortex, and reveal more about the nature of the cortical reorganization.

Whereas we used responses to single tones as the stimulus in this study, AC neurons generally respond to more complex sounds in a manner which is not well explained by the single-tone responses (Ahrens et al., 2008; Carruthers et al., 2013). Our methods could be used to probe the fidelity of cortical representation and behavior in response to any parameterized space of auditory stimuli, e.g. auditory textures, phonemes, or overtone profiles. Similarly to work in visual texture perception (Tkacik et al., 2010; Hermundstad et al., 2014), one could test the discrimination thresholds along different dimensions of the texture space. Changes in these thresholds due to

optogenetic circuit manipulation could then be compared with changes in a neurometric threshold based on Fisher Information, as developed here. Such studies will elucidate the role of AC in facilitating complex auditory discrimination.
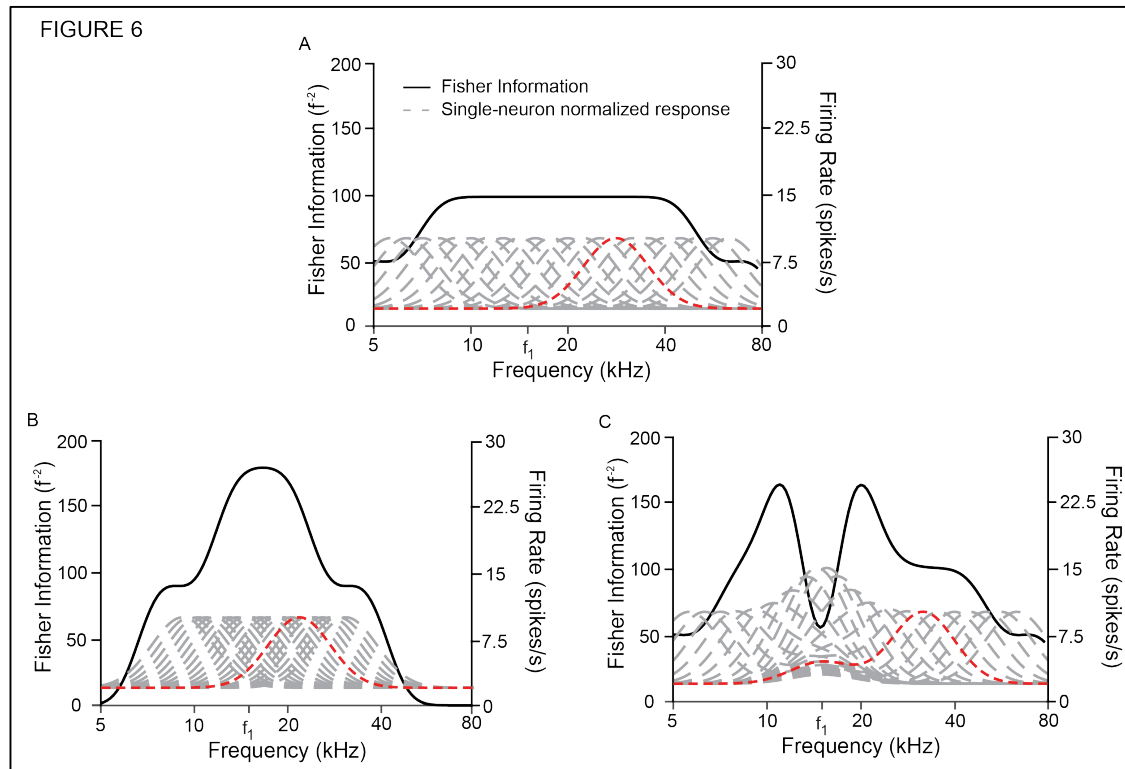

Figure 6. Overrepresenting a specific frequency can increase or reduce sensitivity to that frequency.
A. Fisher information (black) computed from a homogeneous population of neurons (responses in gray) has an even sensitivity across a broad range of frequencies. A sample tuning curve (red) is used to illustrate neural transformations in **B** and **C**. Neurons have baseline activity of 2 spikes/s, peak response of 10 spikes/s, peak frequency spaced 1/20th of a decade apart, with HWHM of .1 decades.
B. Fisher information is plotted for a neural population overrepresenting frequency f_1 by shifting peak frequencies halfway between their original location in **A** and f_1. Fisher information approximately doubles near f_1, but is reduced near the edges.
C. Fisher information is plotted for a neural population overrepresenting frequency f_1 by adding a Gaussian bump near f_1 with an amplitude that diminishes with distance between the preferred frequency of the neuron and f_1. Fisher information is *diminished* at f_1, leading to reduced sensitivity at this frequency, despite its overrepresentation within the population firing activity.

Viewed in aggregate in terms of a mean over individuals, our results would have yielded small average effects with large individual variations appearing as "noise". Averaging in this way would have obscured the function of AC in frequency discrimination because the correlation between individual circuit changes and individual behavioral changes would have been missed. It is only by treating the mice as individuals that we were able to understand the general role auditory cortex plays in shaping the response. We suggest that such attention to individual variation will be broadly

important throughout neuroscience as large-scale recordings begin to reveal the neural basis of behavioral diversity.

Methods.

Animals. All experiments were performed in adult male mice (supplier - Jackson Laboratories; age, 12-15 weeks; weight, 22-32 g; PV-Cre mice, strain: B6; 129P2-Pvalbtm1(cre)Arbr/J; CamKIIα-Cre: B6.Cg-Tg(CamKIIα-Cre)T29-1Stl/J) housed at 28° C on a 12h light:dark cycle with water and food provided *ad libitum*, 5 or fewer animals per cage. All animal work was conducted according to the guidelines of University of Pennsylvania IACUC and the AALAC Guide on Animal Research. Anesthesia by isofluorane and euthanasia by carbon dioxide were used. All means were taken to minimize the pain or discomfort of the animals during and following the experiments. Experiments were performed as described previously (Aizenberg et al., 2015).

Experimental methods overview. Methods have been previously described (Aizenberg et al., 2015). Briefly, at least 10 days prior to the start of experiments, mice were injected with a viral construct, if any, and implanted with optical cannulas, and a headpost, as previously described, under isoflurane anesthesia. Viral construct injection targeted AC using stereotaxic map. Fiber-optic cannulas were implanted bilaterally over the injection site at depth of 0.5 mm from the scull surface. We previously showed that injection of control vectors (modified AAV vectors encoding only GFP or tdTomato under FLEX promoter) in the previous study (Aizenberg et al., 2015) did not drive significant changes in behavioral frequency discrimination acuity, demonstrating that the effect of viral injections on behavior was specific to Arch or ChR2 activation. After recovery, mice were habituated to the head-fixing apparatus, and subjected to behavioral frequency discrimination tests for 1-3 days, followed by electrophysiological recordings in the auditory cortex. On half of the trials in behavioral and neurophysiological recordings, light was presented through the fiber-optic cannula to activate or suppress target neurons. Upon conclusion of experiments, brains were extracted, fixed and subjected to immunostaining for verification of expression of the virus and the target neuronal promoter.

Behavioral frequency discrimination. Behavioral frequency discrimination was measured using a modified PPI procedure on daily basis (Clause et al., 2011; Aizenberg et al., 2015). As previously reported (Aizenberg and Geffen, 2013; Aizenberg et al., 2015), PPI provides psychometric response curves for frequency discrimination over the course of a single session that lasts less than 1 h and does not require training the subject, which can confound interpretation of fear conditioning. Mice were head-fixed, connected to optical cannulas as needed, and placed on a load-bearing platform. Sound was presented through a speaker, consisting of a background tone (15kHz, 10-20 s) that, on each trial, switched to a pre-pulse tone (10.2, 12.6, 13.8, 14.7, and 15.0 kHz, 60 ms) followed by startle noise (SS, broad-band noise, 100 dB SPL, 20 ms). The frequency difference between the background and pre-pulse tone is denoted Δf. Each pre-pulse tone was repeated in a pseudo-random order at least 5 times during each behavioral session. The Acoustic Startle Response (ASR) for a given Δf was computed as the average over trials of the difference between the maximum vertical force applied within the 500 ms window following SS and the average baseline activity during 500 ms prior to SS. In each PPI session, the PPI was calculated as:

Page 16

$$PPI(\Delta f) = 100 \frac{ASR(0) - ASR(\Delta f)}{ASR(0)}$$

where PPI is measured in %, and $ASR(\Delta f)$ is measured using the 50% of the strongest ASR magnitudes for each PP frequency. 50% is chosen for consistency with previous work, as the psychometric curve has the steepest slope at this value (Aizenberg and Geffen, 2013). Weaker ASR magnitudes were rejected to avoid confounds from animal motion. Behavioral threshold was determined by fitting the PPI with a generalized logistic function, and defining the threshold for the fit as the Δf that produced 50% of the maximum PPI. Because the primary source of uncertainty related to how close the animal's threshold was to sampled points, we computed thresholds for the set of fits producing less than a 25% increase in MSE relative to the best fit (although increasing this cutoff to 60% yielded small differences). We took the mean and standard deviation of the resulting set of thresholds to reflect the animal's threshold. Each psychometric functions consisted of 5 data points representing the difference between the background frequency and 5 prepulse frequencies (PP). Each data point was obtained by averaging ASRs from all repetitions corresponding to a given frequency. In a standard PPI session, 20 repetitions of each PP were presented (100 trials in total). However, if either threshold was out of the range (0.5–32%) or the fit coefficient of the curve (R^2) was below 0.7, the mouse underwent an additional 10 repetitions (50 trials). If threshold and fit curve failed to meet the above criteria after 200 trials, the session was excluded from statistical analysis (3 out of 61 sessions). Previous studies have shown that psychometric thresholds obtained from day-to-day measurements were stable (Aizenberg and Geffen, 2013; Aizenberg et al., 2015; Mwilambwe-Tshilobo et al., 2015). Light-on trials included a 1s laser presentation that starts 0.5 s preceding PP onset. Light-off trials included laser presentation at quasi-random position during ITI. All analysis was performed separately on light-on and light-off trials. Simple randomization was used to assign the subjects to the experimental groups. A pseudorandom sequence was used for tone presentation during PPI tests. During PPI procedure, the timing of the laser presentation on Laser-off trials was pseudo-randomized with respect to the timing of the tones. Blinding of experiment with respect to animal groups was not possible as animals in different groups underwent different experimental protocols.

Neuronal tone response measurement. All recordings were carried out inside a double-walled acoustic isolation booth (Industrial Acoustics) as previously described (Aizenberg et al., 2015). Activity of neurons in the primary auditory cortex of head-fixed, awake mice was recorded via a silicon multi-channel probe (Neuronexus). Viral construct was injected, targeting AC using a stereotaxic map. Fiber-optic cannulas were implanted bilaterally over the injection site at depth of 0.5 mm from the skull surface. Viral spread was confirmed postmortem by visualization of the fluorescent protein expression in fixed brain tissue, and its co-localization with PV or excitatory neurons, following immuno-histochemical processing with the appropriate antibody. Putative principal (excitatory) neurons were identified using waveform and spontaneous firing rate (for details see (Aizenberg et al., 2015)). Acoustic stimulus was delivered via a calibrated magnetic speaker (Tucker-Davis Technologies) (Carruthers et al., 2013). We measured the frequency tuning curves by presented a train of 50 pure tones (50ms long, ISI 450 ms) with frequencies spaced logarithmically between 1 and 80 kHz and at 8 intensities (sound pressure levels, SPLs) spaced uniformly between 10 and 80 dB, a standard

procedure in characterizing auditory responses, and determined the threshold amplitude for tone at each frequency for each neuron (Carruthers et al., 2013; Aizenberg et al., 2015). For data analysis we averaged responses of the neurons to each tone across 3 highest amplitudes. Each tone was repeated twice in pseudo-random sequence and the stimulus was counter-balanced for laser presentation. On light-on trials, light was presented via the optic cannulas, with the onset of 100 ms prior to tone onset, and lasting for 250 ms. The full stimulus was repeated 5 times.

Histology. Virus spread was confirmed postmortem by visualization of the fluorescent protein expression in fixed brain tissue, and its colocalization with PV or excitatory neurons, following immuno-histochemical processing with the appropriate antibody.

Identification of Putative Excitatory Neurons. Putative principal (excitatory) neurons were identified using waveform and spontaneous firing rate (for details see Aizenberg et al., 2015).

Neural Response Analysis. The neural frequency response function was calculated using the average frequency tuning curve across the three highest intensities. The results was modeled using a Gaussian in log-frequency space:

$$FR(f) = B + A * \exp\left[-\frac{(f - f_0)^2}{2\sigma^2}\right]$$

where B represents the baseline response, A represents the amplitude of the strongest evoked response (relative to baseline), f_0 represents the frequency evoking the strongest response, and σ corresponds to the width of the frequency response function. Only neurons whose Gaussian fit had $R^2 > .6$ were kept for further analysis.

In order to calculate Fano factor of a neuron, we calculated mean and variance of the firing rate to each combination of frequency and SPL. The slope of these data was taken as an estimate of Fano factor.

The correlation between neurons (calculated only between simultaneously recorded neurons) was computed using a reduced measure of deviation from the mean for each neuron:

$$s_i^k(f, d) = \frac{r_i^k(f, d) - \overline{r_i}(f, d)}{\sqrt{F_i \overline{r_i}(f, d)}}$$

where k denotes the repetition number (1-5), i denotes the neuron, f denotes the frequency, d denotes the intensity, r denotes the evoked response, $\bar{r}$ denotes the average response (firing rate) of a neuron to a particular frequency and intensity, and F denotes the Fano factor of that neuron. For a generalized Poisson process, s_i has zero mean and unit variance because the variance is proportional to the mean. The correlation between two neurons is then given by

$$C_{i,j} = \langle s_i^k(f, d) s_j^k(f, d) \rangle_{k,f,d}$$

Computing Fisher Information. Fisher information was calculated to provide a measure of neurometric frequency discrimination. Fisher information was calculated numerically from the recorded data based on the characterization of the neural responses (see *Neural Response Analysis*), and is given by:

$$I_F(f) = \sum_{\vec{n}} P(\vec{n}|f) \left(\frac{\partial}{\partial f} \log P(\vec{n}|f) \right)^2$$

where P is the probability that the population of neurons produces $\vec{n} = (n_1, n_2, ...)$ spikes in response to the tone f. Assuming Poisson variability and independent neurons,

$$P(\vec{n}|f) = \prod_i P(n_i|f) = \prod_i \frac{e^{-\mu_i(f)}\mu(f)^{n_i}}{n_i!}$$

where the first equation expresses the independent neuron assumption and the second step uses the assumption of Poisson variability. Here, μ_i and n_i are the expected and observed number of spikes from neuron i, respectively. A second model assumes independent neurons and uses a generalized Poisson distribution:

$$P(n_i|f) = \frac{\alpha_i(f)(\alpha_i(f) + n_i\lambda_i)^{n-1}e^{-(\alpha_i(f)+n_i\lambda_i)}}{n_i!}$$

where $\alpha_i = \mu_i(f) * F_i^{-1/2}$ and $\lambda_i = 1 - F_i^{-1/2}$. This model only allows for Fano factors above 1, which is consistent with other models of neural variability and measured cortical variability (Goris et al., 2014; Blackwell et al., 2016). We therefore set any measured Fano factor less than 1 to exactly 1 for the purpose of the Fisher information calculation.

Estimating the number of neurons for neurometric thresholds. Animals displayed varying levels of frequency discrimination acuity, and we measured different sized subsets of frequency-tuned neurons in each experiment. In order to estimate the number of neurons required to account for behavioral discrimination acuity from the measured population, we utilized the fact that Fisher information for a population of independent neurons is the sum of the Fisher information from each neuron.

$$I^{(total)} = \sum_n I^{(n)}$$

We then assume that the population of neurons that we measured are representative of the overall population (at least the population that contributes to discrimination at the relevant frequency).

$$I^{(n)} \approx \frac{1}{N_E} \sum_{k=1}^{N_E} I_E^{(k)} = \frac{1}{N_E} I_E^{(total)}$$

Here we use n to refer to the overall population that we seek to estimate, k to index the neurons that were measured, N_E is the number of frequency-tuned neurons measured in a specific mouse, $I_E^{(k)}$ is the Fisher information of these experimentally measured neurons, and $I_E^{(total)}$ is the total information used to calculate the neurometric threshold. Recalling that the neurometric threshold is defined as $I^{-1/2}$, we then have

$$I^{(total)} = \frac{N_T}{N_E} I_E^{(total)}$$

We can rewrite this as

$$N_T = N_E \left(\frac{t_{beh}}{t_{neu}} \right)^2$$

Page 19

where t_{beh} is this behaviorally measured threshold and t_{neu} is the neurometric estimate of the threshold. This is plotted for each animal used in our analyses in Figure 4 – Figure Supplement 2, and we find that the average for both light-on and light-off conditions is just about 10^3 neurons.
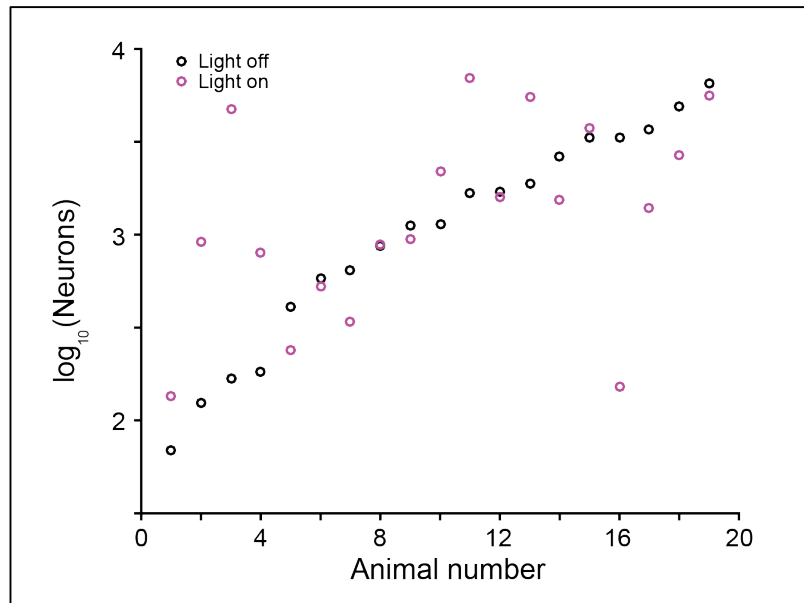

Figure 4 – Figure Supplement 2: Number of frequency-tuned neurons required to account for behavioral sensitivity for each mouse. Average of both light-on and light-off conditions is ~10^3 neurons.

Comparing behavioral and neurometric thresholds. Neural responses were accumulated over all recording sessions for each mouse, and used to compute the Fisher information for the animal. The Fisher information provides a bound on the variability of an unbiased estimator, and any criterion level of decoding performance scales with the inverse-square root of the Fisher information. If neural responses are independent, the Fisher information scales linearly with the number of neurons. In order to compare threshold predictions between mice with different numbers of measured neurons, we computed the average Fisher information per neuron. This allowed us to compare across mice and to estimate the minimum number of effective frequency-tuned neural units that must contribute to explain the observed frequency discrimination performance(Cover and Thomas, 1991). To estimate the neurometric threshold, we first computed the inverse square root of the Fisher information per neuron, and took an average over a small region around 15 kHz (the baseline frequency used in behavioral tests). Only mice with more than 10 recorded frequency-tuned neurons were included in the analysis (19 mice). Our estimate is a lower limit on the uncertainty in the estimate of this tone frequency based on the recorded population responses. Since Fisher information scales linearly in an independent population, this method also provides an estimate on the effective number of neurons, which must contribute to the tone representation in order to account for behavioral discriminability (Figure 7). The observed neurometric discriminability with order one thousand independent neurons is similar to behavioral discrimination acuity.

Data availability. All relevant data will be deposited in the Dryad database and made publically available.

Code availability. All relevant code will be posted on Github and made publically available.

Page 20

References

Ahmadian Y, Pillow JW, Paninski L (2011) Efficient Markov chain Monte Carlo methods for decoding neural spike trains. Neural Comput 23:46-96.

Ahrens M, Linden J, Sahani M (2008) Nonlinearities and contextual influences in auditory cortical responses modeled with multilinear spectrotemporal methods. J Neurosci 28:1929-1942.

Aizenberg M, Geffen MN (2013) Bidirectional effects of auditory aversive learning on sensory acuity are mediated by the auditory cortex. Nature neuroscience 16:994-996.

Aizenberg M, Mwilambwe-Tshilobo L, Briguglio JJ, Natan RG, Geffen MN (2015) Bidirectional Regulation of Innate and Learned Behaviors That Rely on Frequency Discrimination by Cortical Inhibitory Neurons. PLoS Biol 13:e1002308.

Bakin JS, Weinberger NM (1990) Classical conditioning induces CS-specific receptive field plasticity in the auditory cortex of the guinea pig. Brain Res 536:271-286.

Blackwell JM, Taillefumier TO, Natan RG, Carruthers IM, Magnasco MO, Geffen MN (2016) Stable encoding of sounds over a broad range of statistical parameters in the auditory cortex. Eur J Neurosci 43:751-764.

Carruthers IM, Natan RG, Geffen MN (2013) Encoding of ultrasonic vocalizations in the auditory cortex. J Neurophysiol 109:1912-1927.

Chen QC, Jen PH (2000) Bicuculline application affects discharge patterns, rate-intensity functions, and frequency tuning characteristics of bat auditory cortical neurons. Hear Res 150:161-174.

Churchland MM et al. (2010) Stimulus onset quenches neural variability: a widespread cortical phenomenon. Nat Neurosci 13:369-378.

Clause A, Nguyen T, Kandler K (2011) An acoustic startle-based method of assessing frequency discrimination in mice. J Neurosci Methods 200:63-67.

Cover TM, Thomas JA (1991) Elements of Informatioin Theory. New York: Wiley.

de la Rocha J, Marchetti C, Schiff M, Reyes AD (2008) Linking the response properties of cells in auditory cortex with network architecture: cotuning versus lateral inhibition. J Neurosci 28:9151-9163.

Dror G, Tsodyks M (2000) Activity of coupled excitatory and inhibitory neural populations with dynamic synapses. Neurocomputing 32-33:359-364.

Fritz J, Shamma S, Elhilali M, Klein D (2003) Rapid task-related plasticity of spectrotemporal receptive fields in primary auditory cortex. Nat Neurosci 6:1216-1223.

Fritz JB, Elhilali M, Shamma SA (2005) Differential dynamic plasticity of A1 receptive fields during multiple spectral tasks. J Neurosci 25:7623-7635.

Froemke RC (2015) Plasticity of cortical excitatory-inhibitory balance. Annu Rev Neurosci 38:195-219.

Froemke RC, Carcea I, Barker AJ, Yuan K, Seybold BA, Martins AR, Zaika N, Bernstein H, Wachs M, Levis PA, Polley DB, Merzenich MM, Schreiner CE (2013) Long-term modification of cortical synapses improves sensory perception. Nat Neurosci 16:79-88.

Gimenez TL, Lorenc M, Jaramillo S (2015) Adaptive categorization of sound frequency does not require the auditory cortex in rats. J Neurophysiol 114:1137-1145.

Goris RL, Movshon JA, Simoncelli EP (2014) Partitioning neuronal variability. Nat Neurosci 17:858-865.

Gu Y, Fetsch CR, Adeyemo B, Deangelis GC, Angelaki DE (2010) Decoding of MSTd population activity accounts for variations in the precision of heading perception. Neuron 66:596-609.

Hermundstad AM, Briguglio JJ, Conte MM, Victor JD, Balasubramanian V, Tkacik G (2014) Variance predicts salience in central sensory processing. Elife 3.

Kilgard MP, Merzenich MM (2002) Order-sensitive plasticity in adult primary auditory cortex. Proc Natl Acad Sci U S A 99:3205-3209.

Kurt S, Ehret G (2010) Auditory discrimination learning and knowledge transfer in mice depends on task difficulty. Proc Natl Acad Sci U S A 107:8481-8485.

Li LY, Xiong XR, Ibrahim LA, Yuan W, Tao HW, Zhang LI (2015) Differential Receptive Field Properties of Parvalbumin and Somatostatin Inhibitory Neurons in Mouse Auditory Cortex. Cereb Cortex 25:1782-1791.

Moore AK, Wehr M (2013) Parvalbumin-expressing inhibitory interneurons in auditory cortex are well-tuned for frequency. J Neurosci 33:13713-13723.

Mwilambwe-Tshilobo L, Davis AJ, Aizenberg M, Geffen MN (2015) Selective Impairment in Frequency Discrimination in a Mouse Model of Tinnitus. PLoS One 10:e0137749.

Natan RG, Briguglio JJ, Mwilambwe-Tshilobo L, Jones SI, Aizenberg M, Goldberg EM, Geffen MN (2015) Complementary control of sensory adaptation by two types of cortical interneurons. eLife 4:pii: e09868.

Ohl FW, Wetzel W, Wagner T, Rech A, Scheich H (1999) Bilateral ablation of auditory cortex in Mongolian gerbil affects discrimination of frequency modulated tones but not of pure tones. Learn Mem 6:347-362.

Oswald AM, Schiff ML, Reyes AD (2006) Synaptic mechanisms underlying auditory processing. Curr Opin Neurobiol 16:371-376.

Ozeki H, Finn IM, Schaffer ES, Miller KD, Ferster D (2009) Inhibitory stabilization of the cortical network underlies visual surround suppression. Neuron 62:578-592.

Phillips EA, Hasenstaub AR (2016) Asymmetric effects of activating and inactivating cortical interneurons. Elife 5.

Polley D, Steinberg E, Merzenich M (2006) Perceptual learning directs auditory cortical map reorganization through top-down influences. J Neurosci 26:4970-4982.

Recanzone GH, Merzenich MM, Schreiner CE (1992) Changes in the distributed temporal response properties of SI cortical neurons reflect improvements in performance on a temporally based tactile discrimination task. J Neurophysiol 67:1071-1091.

Recanzone GH, Schreiner CE, Merzenich MM (1993) Plasticity in the frequency representation of primary auditory cortex following discrimination training in adult owl monkeys. J Neurosci 13:87-103.

Rudy B, Fishell G, Lee S, Hjerling-Leffler J (2011) Three groups of interneurons account for nearly 100% of neocortical GABAergic neurons. Dev Neurobiol 71:45-61.

Schuz A, Palm G (1989) Density of neurons and synapses in the cerebral cortex of the mouse. J Comp Neurol 286:442-455.

Seybold BA, Phillips EA, Schreiner CE, Hasenstaub AR (2015) Inhibitory Actions Unified by Network Integration. Neuron 87:1181-1192.

Talwar SK, Gerstein GL (2001) Reorganization in awake rat auditory cortex by local microstimulation and its effect on frequency-discrimination behavior. J Neurophysiol 86:1555-1572.

Tan AY, Wehr M (2009) Balanced tone-evoked synaptic excitation and inhibition in mouse auditory cortex. Neuroscience 163:1302-1315.

Tkacik G, Prentice JS, Victor JD, Balasubramanian V (2010) Local statistics in natural scenes predict the saliency of synthetic textures. Proc Natl Acad Sci U S A 107:18149-18154.

Tramo MJ, Shah GD, Braida LD (2002) Functional role of auditory cortex in frequency processing and pitch perception. J Neurophysiol 87:122-139.

Tsodyks MV, Skaggs WE, Sejnowski TJ, McNaughton BL (1997) Paradoxical effects of external modulation of inhibitory interneurons. J Neurosci 17:4382-4388.

Wang J, Caspary D, Salvi RJ (2000) GABA-A antagonist causes dramatic expansion of tuning in primary auditory cortex. Neuroreport 11:1137-1140.

Wang J, McFadden SL, Caspary D, Salvi R (2002a) Gamma-aminobutyric acid circuits shape response properties of auditory cortex neurons. Brain Res 944:219-231.

Wang J, McFadden SL, Caspary D, Salvi R (2002b) Gamma-aminobutyric acid circuits shape response properties of auditory cortex neurons. Brain Res 944:219-231.

Wehr M, Zador AM (2003) Balanced inhibition underlies tuning and sharpens spike timing in auditory cortex. Nature 426:442-446.

Wu GK, Arbuckle R, Liu BH, Tao HW, Zhang LI (2008) Lateral sharpening of cortical frequency tuning by approximately balanced inhibition. Neuron 58:132-143.

Znamenskiy P, Zador AM (2013) Corticostriatal neurons in auditory cortex drive decisions during auditory discrimination. Nature 497:482-485.